Piezoelectric dual axis cantilever force measurement probe

Juhani Virtanen, Arno Pammo, Antti Vehkaoja, *Member IEEE*, and Sampo Tuukkanen
Faculty of Medicine and Health Technology, Tampere University (TAU) Tampere, Finland

Abstract—**A piezoelectric cantilever force sensor consisting of a mechanical cantilever probe, an analog amplifier and an embedded digital signal processing unit is presented. The sensor is constructed from a lead zirconate titanate (PZT) piezo disc, which was cut into four segments and a 33-mm-long metal probe attached to it perpendicularly to the piezo disc plane. The signal of the piezoelectric elements was amplified with a four channel operational amplifier circuit having voltage gain of 10 (20 dB) in each channel and input resistance of 50 MΩ. The digital signal processing was implemented on an Arduino Due -based hardware. Signal pre-processing block consists of three cascaded digital infinite impulse response (IIR) filters were composed: A DC-blocking filter, a notch filter and a low pass filter. Additionally, a moving average filter was implemented to further enhance the system tolerance to power line interference and to reduce the sampling rate to 50 Hz. Finally, a LabVIEW software is used to provide an interface for the Arduino Due. The calibration of the system was carried out with a texture analyzer and it was capable of sensing biaxial forces in the range of 2 millinewton with a RMS error of less than 60 micro Newton and hysteresis in the order of 0.25 millinewton or 12.5% of the full scale reading. Cross talk ratio between axes was 25.3 or 28.0 in dB. The applicable force measurement frequency range was 0.5 – 10 Hz.**

Keywords—Force measurement, dual axis, piezoelectric

I. Introduction

During recent two decades, there has been an increasing trend towards miniaturization and micromanipulation in many fields, such as biomedical engineering, robotics, industrial automation and materials sciences. In the miniaturized systems, force measurement becomes critical not only due to the small forces to be measured but also because the miniaturized equipment are easily damaged [1]. The force sensing solutions range from resonant tactile force sensors for robotic touch sensing, in which the change in the resonant frequency of piezoelectric force sensor changes as a function of applied force [2], to screen printed thick film piezoelectric slip sensor, which is used to enhance the functionality of a prosthetic hand by decreasing the complexity of the touch sensing system [3]. Along with a piezoelectric sensor principle, piezoresistive sensing can be applied in similar sensing applications, except the piezoelectric sensor cannot detect static forces. For example, a screen printed piezoresistive cantilever sensor proposed by Lakhmi *et al*. has shown capability to measure static forces in micronewton range [4].

In addition to varying physical operation principle, different approaches, such as utilizing piezoelectric foils or membranes, are suitable for force sensing. For example, polyvinylidene fluoride (PVDF) based piezoelectric membrane sensors have been proposed for single cell biological force measurements [5] or in defining mechanical properties such as shear strength of paper fiber [6]. Further, sensors processed on a silicon wafer are commonly utilized in micro electromechanical systems (MEMS) providing capability down to nanonewton range force sensing [7]. More advanced three-axis silicon membrane based piezoresistive force sensor has been reported to measure forces below micronewton range [8].

However, it should be noted that the low force detection capability in millinewton or smaller scale is not limited solely to piezoelectric or piezoresistive properties. For example, strain gauge-based resistive, capacitive, piezo magnetic, optical, vision-based, and electroactive force sensors have been developed [1]. Common challenge to all low force sensing techniques relying on a linear elastic material property is tailoring the elastic properties of the measurement system such that the actual force measurement dominantly takes place instead of only a displacement or movement observation [1].

Sophisticated low force measurement and manipulation techniques provide interesting opportunities to study and quantify behavior of small scale biological organisms. Recently, there has been increasing interest towards *in vitro* cardiac contraction force measurement for engineered tissues. Regarding the utilization of piezoresistive sensing principle, Sasaki *et al*. proposed a force measurement approach based on cell construct cultivation on a specific fibrin sheet “cell sheet engineering” [9] and Wang *et al*. reported utilization of an elastic sheet with carbon nanotubes (CNT) [10]. Linder *et al*. demonstrated pressure based force sensing by using an elastic membrane with a gas chamber and a pressure sensor “cell drum technology” [11]. Mannhardt *et al*. reported a force measurement based on optical analysis of a cell structure cultured between two adjacent bending beams [12]. There are several reports about utilization of atomic force microscope (AFM) cantilever for a direct contraction force measurement [13-15]. Similarly, Gaitas *et al*. reported a direct cardiomyocyte contractile force measurement based on piezoresistive sensor embedded on a polyimide micro cantilever arrangement [16].

In our previous work, we have developed a customized single axis cantilever force measurement technique, which is composed of one sensing element [17]. Here, we present a dual axis approach which is based on piezoelectric four-element sensor attached to a metallic cantilever capable of

sensing forces in two directions. In the previous work, we are limited to measurement of force in only one direction, which places a challenge on proper alignment of the measurement probe. In the engineered tissues the tissue structures and cells are often randomly oriented requiring the contraction force measurement orientate accordingly. In this application it would be beneficial to have at least two axis force sensing capability. The dual axis force measurement capability enables positioning of the measurement probe tip to an area of interest without having to accurately align it with contraction direction. Thus making the force measurement incur better repeatability. This type of biomeasurement can be used to study for example toxicity of potential drugs before moving to clinical phase in the drug development. From the ethical point of view, the amount of animal testing could be reduced with this approach.

Open source hardware development platform such as Arduino [18-20], provide cost effective and versatile alternative for implementation of various embedded electronic measurement systems with low costs. For example a range of customizable biomeasurement instrumentation can be built onto these kind of platforms reducing a black box problem where the operation of the measurement devices is not completely understood by the developer.

In this work, a dual axis force measurement system was developed using Arduino Due open source platform and in-house developed piezoelectric cantilever sensor. Our interest was to study the capabilities of this customizable measurement platform with added functionalities such as embedded digital signal processing and to study the performance of the piezoelectric dual axis cantilever force sensor performance.

II. Materials and Methods

A piezoelectric cantilever based force measurement system, consisting of a piezoelectric dual axis mechanical cantilever probe, an analog voltage amplifier and a digital signal processing unit, was developed for applications requiring sub-mN force measurement. A LabVIEW (National Instruments corporation, Austin, USA) user interface program was developed for further processing, visualization and storing of the measurement data.

A. The dual axis force measurement probe sensor

The cantilever probe arrangement was constructed from a 15 mm diameter lead zirconate titanate (PZT) piezo disc that was first cut into four symmetric segments. The cutting was done with a rotary diamond cutting disc. The sensing segments are labeled from E1 to E4. The schematic sensor arrangement is illustrated in the in Fig. 1. Further a 33 mm long metal cantilever probe pointing at *z*-direction was attached in the middle of the segment apexes perpendicularly to the piezo disc plane. The attachment was done by soldering the probe to the piezo disc. Being significantly thicker than the piezo disc, the joint was considered to be much firmer than the piezo disc, thus not affecting the force measurement results. Further, the segments were fixed to a printed wiring board (PWB) frame in *xy*-plane from the opposite sides to the apexes. When a radial force is applied to the cantilever tip, stress is induced to the piezoelectric elements. This results in charge separation in the piezo elements which then can be measured as voltage output using the voltage amplifier. Depending on the force direction, the stress applied to the different piezo elements changes, resulting to a separation of forces in *x* and *y* -directions. To some extent, this kind of construction is also capable of sensing *z*-directional forces but this was not in the interest of this study. The working principle of the force sensor is similar to what has been presented earlier in [17, 21-23].

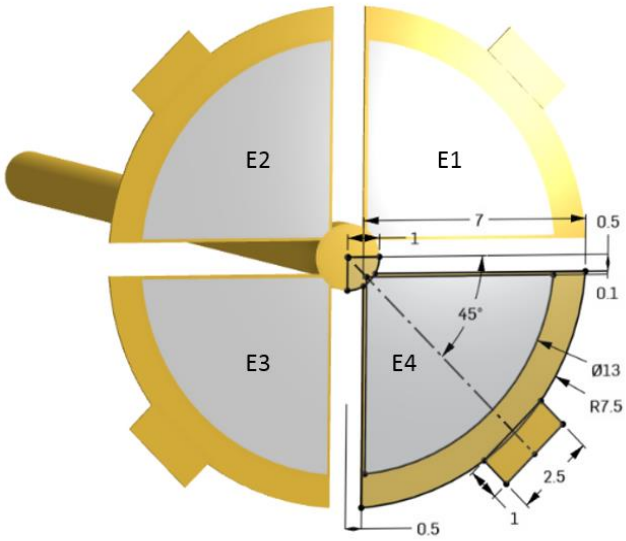

Fig. 1. The piezoelectric cantilever sensor probe. All measures are given in millimeters. (Figure adapted from reference: [18]).

The sensor functionality was first simulated with a finite element method (FEM) (COMSOL Multiphysics, Stockholm, Sweden). This simulation involved a linear elastic physics model simulation combined with a piezoelectric model. This FEM model was used to compute the displacement and electrical field at 2 mN static load at the probe tip to represent the maximum output amplitude in an electrically unloaded situation. This information was then used to compute the spring constant and sensitivity estimates for the sensor. The sensitivities and spring constants were computed in both 0-degree and 45-degree orientation. The potential field in 0-degree results are shown in Fig. 2a and the electric potential field in 45-degree orientation in Fig. 2b. It was also confirmed with FEM simulation that *z*-axis load does only have a negligible effect (less than 0.01 %) on the *xy*-plane force measurement results.

The actual *x* and *y* force components are computed as a linear combination of the sensor element signals. This is done is such way that the components divided by the axis of interest are first weighted with opposing signs and then integrated. The resulting formulas are presented in (1) for *x*-axis and (2) for the *y*-axis.

$$x = (E1+E4) - (E2+E3) \quad (1)$$

$$y = (E1+E2) - (E3+E4) \quad (2)$$

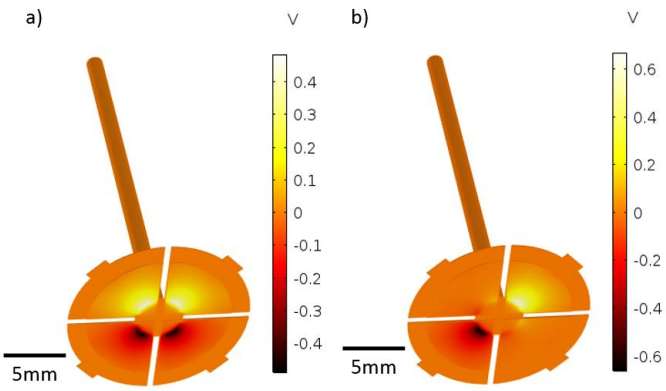

Fig. 2. Electric potential field for 2 mN load in a) 0 degrees orientation b) 45 degrees orientation.

A frequency response simulation was also carried out to obtain parameters for a second order mechanical resonator model. The natural frequency and the damping factor were obtained from the frequency response simulation. The usable frequency band was initially computed from the numerical model and later confirmed with actual impulse response measurements. The analytical model for cantilever transfer function is shown in Equation 3. It represents a second order mechanical system response characterized with a natural frequency (ω_0) and a damping factor (ζ). From the simulation a ω_0 of 1330 rad/s (212 Hz) and a zeta of 0.37 was obtained. Thus, it was concluded that the resonance of the cantilever system is outside of the desired measurement frequency band of approximately from 0.5 to 10 Hz.

$$H(s) = \frac{{\omega_0}^2}{s^2 + 2\zeta\omega_0 s + {\omega_0}^2} \qquad (3)$$

B. *The measurement hardware*

A four channel analog voltage amplifier circuit was designed to interface the force sensor segments. This amplifier output was sampled with 12-bit analog to digital converter (ADC) of the Arduino board. Each channel of the analog front-end consisted of a voltage amplifier with voltage gain of 20 dB (10x). The input resistance of the amplifier was 50 MΩ. This input was driven directly by the piezo disc transducer having 2.5 nF capacitance. This arrangement described in Fig. 3 resulted a high pass behavior of the piezo sensor with pole frequency of 1.27 Hz.

The amplifier circuit was implemented with AD8691 (Analog Devices incorporated, Norwood, USA) precision operational amplifiers. Moreover, the amplifier had a first order low pass filter with a cut off frequency of 40 Hz to reduce the overall noise and prevent aliasing. An analytical model of the transfer function of the amplifier was constructed and this was later used to analyze the total behavior along with the other transfer functions. The values of the discrete components of the amplifier are listed in Table I.

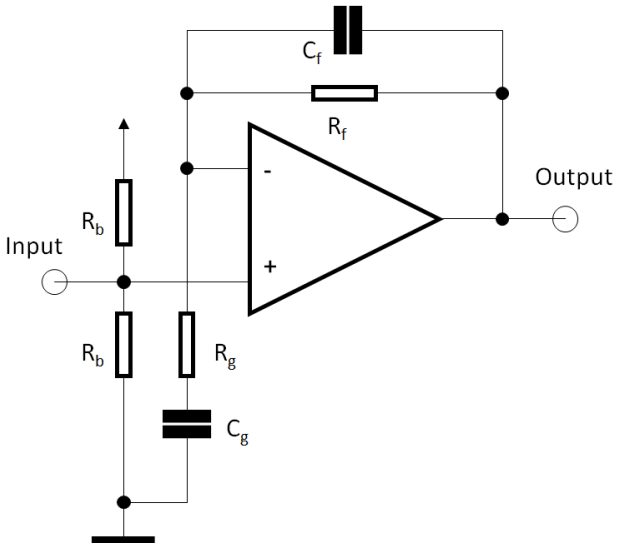

Fig. 3. Front-end amplifier schematic.

TABLE I. Component values of the front-end amplifier.

Component	R_b	R_g	C_g	R_f	C_f
Value	100 MΩ	100 kΩ	10 µF	0.91 MΩ	4.7 nF

The transfer function of the amplifier is shown in Equation 4.

$$A(s) = \frac{R_f}{(R_f C_f s + 1)} \cdot \frac{C_g s}{(R_g C_g s + 1)} \qquad (4)$$

A photograph of the PWB of the sensor-amplifier is shown in Fig. 4. The top side sensor PWB with the measurement probe attached to is shown in Fig. 4a, and the bottom side in Fig. 4b.

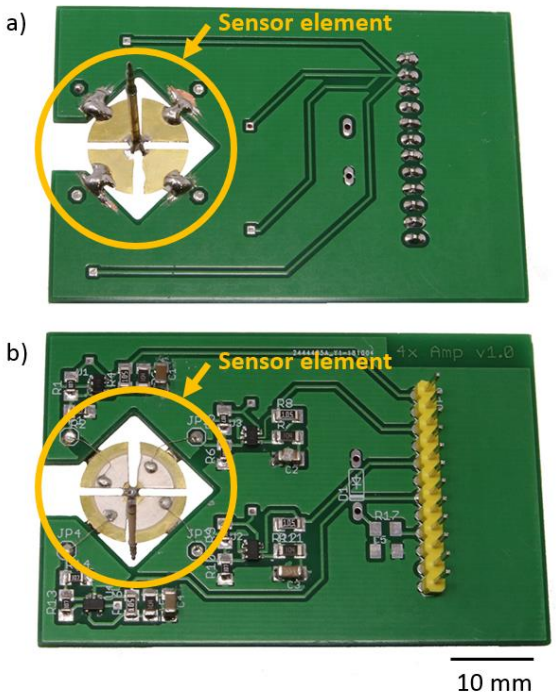

Fig. 4. Photographs of the sensor PWB from a) bottom (sensor) side and b) top (electronics) side.

C. *Digital signal processing*

The signal processing was done using an Arduino Due as the hardware platform. It consists of an Atmel SAM3x8E (Microchip corporation, Chandler, USA) microcontroller having a 32-bit ARM processor architecture operating at 84 MHz clock frequency with a floating point processing unit. In addition, it contains an integrated multiplexed 10 channel 12-bit ADC unit. Moreover, the platform contains a native Universal Serial Bus (USB) communication unit integrated on the chip. The controller and its peripherals are described in more detail in the microcontroller data sheet [24].

The analog four channel signal was first sampled with the Arduino Due with sampling frequency of 3 kHz. This was chosen such that the later the averaging filter would have zeros at 50 Hz and at its harmonic frequencies. This was to remove the most prominent 50 Hz power line interference from the measured signal. An averaging filter was used to reduce the sampling rate to 50 Hz, which was assumed adequate for the proposed application. The reason to down sample the signal was to prepare the measurement system to be able to operate in a large sample quantity measurement simultaneously. For example, a standard cell cultivation well plate may have multiple wells reaching up to several hundred of them, increasing the data flow to the recording and analyzing systems accordingly. The signal was first filtered with three types of digital infinite impulse response (IIR) filters. Initially three IIR filters were composed and later they were cascaded to form a 7th order IIR filter which was then embedded into the Arduino system [25]. The overall transfer function of the IIR filter is shown in (5) while the IIR filter coefficients are shown in Table II.

$$H(z) = \frac{\sum b_n z^{-n}}{\sum a_n z^{-n}} \; ; \; n = [0...7] \qquad (5)$$

TABLE II. 7th order IIR filter coefficients.

Order	A	B
z^{-0}	1	4.3549E-07
z^{-1}	-6.83482	4.4026E-07
z^{-2}	20.03316	-1.2922E-06
z^{-3}	-32.6413	-1.2969E-06
z^{-4}	31.93014	1.2969E-06
z^{-5}	-18.75189	1.2922E-06
z^{-6}	6.12171	-4.4026E-07
z^{-7}	-0.85699	-4.3549E-07

After the IIR filtering, block averaging was applied batch wise to further remove noise and down sample the signal. The other advantage of this procedure is that as the noise in the ADC input is assumed Gaussian distributed, the resolution of the ADC will be increased proportional to the square root of the average length. In this case, the increase is approximately three bits [26, 27]. The amplitude and the phase responses of the combined filter transfer function are shown in Fig. 5.

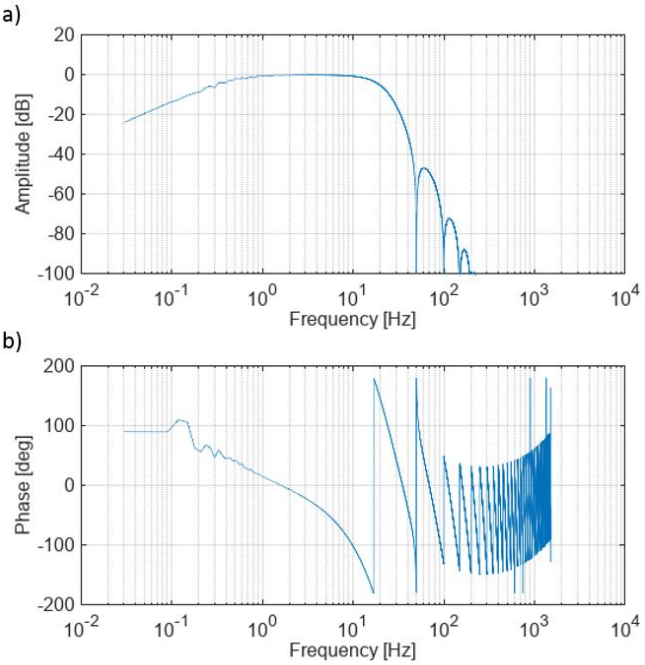

Fig. 5. The Amplitude and phase response of the cascaded filter (figures adapted from reference [18]).

III. RESULTS AND DISCUSSION

A. *Cantilever sensor system impulse response*

The simulation was carried out in frequency domain and the actual measurement in time domain. The time domain impulse response was obtained by creating an impulse-like excitation to the tip of the sensor by tapping it in *xy* -plane direction. The frequency response was then obtained from the time domain measurement of the impulse response by taking a discrete Fourier transform. The sensitivity measurement was then used to match the absolute level of the impulse response. This impulse response data was then further analyzed by computing a discrete Fourier transform (DFT) to obtain frequency response of the cantilever probe. The time domain impulse response is illustrated in Fig. 6a.

Comparison of the measured and simulated amplitude responses are shown in Fig. 6b. Fig. 6 shows good correlation between the simulated and measured amplitude response. In addition, it shows that the frequency range is suitable for low frequency force measurements. Even though the piezoelectric force measurement principle is dynamic in its nature, the force measurement capabilities suit the proposed application. The applicable frequency range of 0.6 – 3.0 Hz has been proposed earlier for cardiac cell contraction force measurement [5].

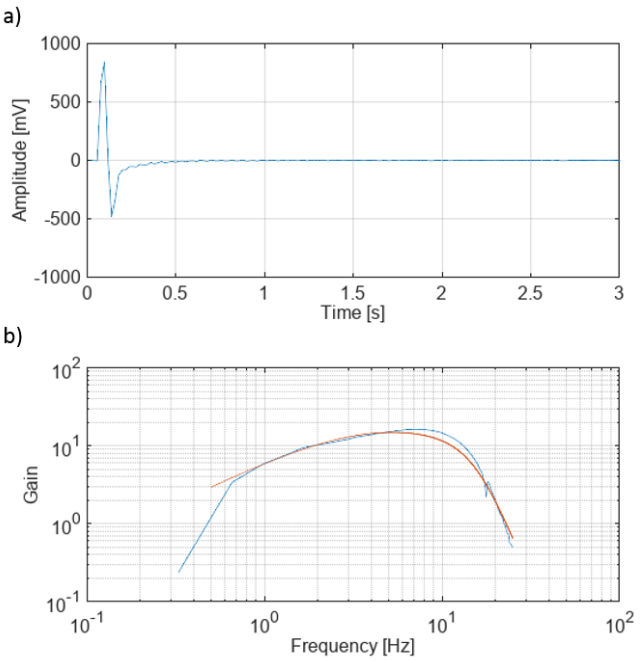

Fig. 6. a) Measured impulse response in time domain. b) Measured (blue) and analytical (red) frequency response of the cantilever sensor system.

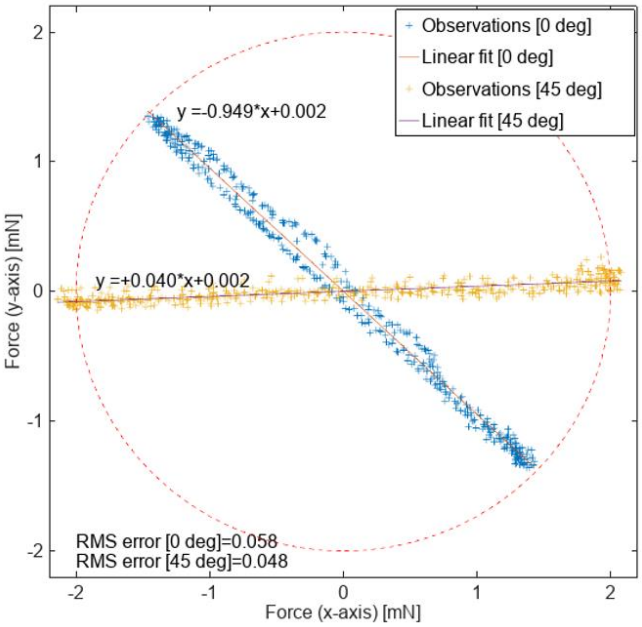

Fig. 7. Calibration results with the measurement observations and their corresponding linear fitted lines. Red circle represents a constant 2 mN load.

B. Calibration and sensitivity measurements

The calibration of the force measurement probe as well as the measurement repeatability analysis was carried out using a TA.XTPlus (Stable Micro Systems Ltd, Surrey, United Kingdom) texture analyzer. The applied calibration method is described in more detail in a previous paper [21]. The procedure consisted of two ±10 µm linear 10 cycle sinusoidal displacement sweeps in *xy*-plane at 0 degrees (*x*-axis direction) and 45 degrees rotated orientation with respect to the *x*-axis. The 10 µm displacement corresponded approximately 2 mN force amplitude. From the calibration data the sensor system sensitivity and the spring constants were computed. The analytical and the measured sensitivity values are listed in Table III. Furthermore, theoretical resolution of the sensor was computed based on the analog-to-digital conversion, which yielded theoretical resolutions of 0.11 µN and 0.12 µN in 0 degrees and 45 degrees orientation, respectively.

The measurement results are presented in Fig. 7. Due to the nature of the in-house assembled prototype sensor there was an orientation error in both of the axes of the piezo sensor elements, which caused systematic error to the sensor readings. Also, the non-optimized alignment of the sensor into 0 and 45 degrees angle with the excitation direction caused some inevitable error to the calibration measurement. However, when the repeatability of the measurement system was studied, it was assumed that this error can be corrected and therefore the repeatability figures were computed relative to the linear fitted axes, which represent in this case the calibration-corrected force excitation directions. The amber and blue scatter plots show the measurement observations. The repeatability computations resulted RMS error of 48 µN in 0 degrees (represented as amber crosses in Fig. 7) and 58 µN in 45 degrees orientation (blue crosses). This corresponds to hysteresis of 0.18 mN and 0.25 mN or 8.75 % and 12.5 % in 0 degrees and 45 degrees orientation respectively. A constant force circle (red) is also drawn in the Fig. 7 to display 2 mN force range.

The sensor output in *x* and *y* -directions were computed in linear combination of all sensor element outputs. The total axis output signals were calculated by adding the potentials on one side (segments E1 and E4 described in Fig. 1 for *x*-signal and segments E1 and E2 described in Fig. 1 for *y*-signal) separated by the axis in interest and subtracting the potentials (segments E1 and E2 in Fig. 1 for *x*-signal and segments E3 and E4 in Fig. 1 for *y*-signal) on the opposing side. There was no axis correlation term used in this calculus. When comparing the maximum deviation in both 0 and 45 degree orientations this shows rather consisted readings suggesting that the sensor design has only small mechanical cross correlation component between *x* and *y* -axes. This result confirmed the sensitivity estimation that was computed in FEM simulation. The crosstalk component is visualized in Fig. 8b. There the excitation has been performed in 45 degree angle. Based on the simulations, the other component should theoretically have been cancelled totally, as the sensor signals should have been equal but opposite. However, due to non-optimized hand-manufactured prototype sensor, this cross correlation component is visible in the measured data presented in Fig. 8b.

In Fig. 8a, combined sensor element output signals are shown when the sensor load is applied at 0 degree angle. There sensor signal component in *x* and *y* -direction are showing similar sized amplitudes in opposite phases. In Fig. 8b, the signals are combined when the load is applied in 45 degree orientation. There the *x* component is much larger than the *y* component. Based on the FEM simulation the individual sensor output components S1 and S3 should cancel each other in this configuration and yield a *y*-component with a zero value. However, with the sensor prototype, this component is clearly measurable and it can be expressed as cross talk between the axes. Here the cross talk is defined as a ratio of the main axis amplitude divided

by the orthogonal axis amplitude. Here the ratio was 25.3 or 28.0 dB.

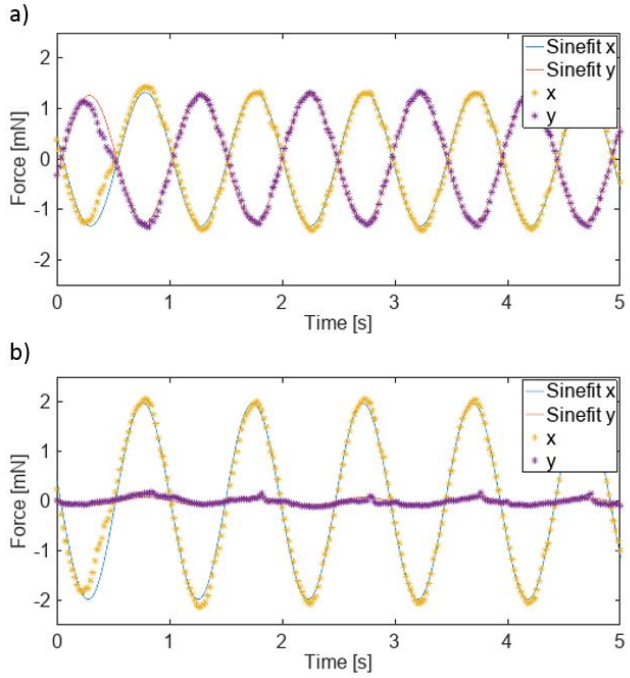

Fig 8. Cross talk (Cross correlation) of a) combined sensor output components in 0 degrees and b) 45 degrees combined signal.

TABLE III. Simulated and measured sensitivities and spring constants.

Parameter	Numerical	Measured
Spring constant 0° [N/m]	209.42	183.08
Sensitivity 0° [V/N]	934.12	932.75
Spring constant 45° [N/m]	209.78	198.48
Sensitivity 45° [V/N]	931.36	826.10

The temperature effect of the sensor was also considered based on literature. It was found that the temperature and humidity have effect on PZT sensitivity [28-31]. However, this was not investigated in this work because especially the proposed biological applications have a high degree of temperature control and used temperature range is small.

As a limitation of the proposed approach, it is noticed that the form factor of the sensor may not be suitable for all proposed applications. For example, the sensor may be too large to be used in single cell level measurements. Also, the operation of the sensor itself is based on linear elastic cantilever, which fixes the spring constant to a certain value. If different mechanical properties are required in the measurement application, the sensor design must be altered accordingly. If miniaturization is desired the sensor electronics and the current PWB approach may not be suitable. In addition, the sensor presented in this work has a prototype nature and the mass production challenges need to be addressed when further developing this force measurement concept. These reasons, and the fact that the sensor is not industrially fabricated but a handmade prototype, are most likely causing large variation in the sensor performance in the case of multiple prototype like sensors are compared. Therefore, certain things such as repeatability was not extensively studied, but the focus was on the sensor design itself. In addition, if for example the repeatability and reproducibility are to be studied in larger context, it involves observing effects such as operator to operator variance. In the future, work on these issues is a very important development aspect and this also involves work on manufacturability to minimize the variance between individual sensor elements. Also, when the sensor fabrication process will be improved to for example reduce sensor-to-sensor variation, it makes it sensible to conduct a series of application measurements and more thorough characterization measurements.

IV. Conclusion

We have demonstrated a dual axis piezoelectric force measurement system capable of measuring forces below 2 mN which was the range of the design input specification. The device studied here has piezoelectric operation principle instead of piezo resistive principle often used in, for example, MEMS sensors. The capability of the developed dual axis force measurement system was demonstrated using an embedded software approach, which provides wide range of possibilities for customized measurement arrangements using open source tools. As an example, measurement of small muscular contraction forces present in in-vitro cardiac tissue constructs is a possible application for the proposed system.

We have also demonstrated an embedded signal processing tool chain with four IIR filters. The filtering successfully removes power line interference and its harmonics from the measurement signal and enables calculating the 2D force components from the four sensor signals. The measurement system was able to carry out 4 channel sampling at 3 kHz sampling frequency and perform the proposed filtering as well as communication with LabVIEW based PC software in real time.

Acknowledgment

This work was funded by the Academy of Finland in the context of “In vitro cardio” -project (grant number 310527) and in the context of “University profiling grant” (grant number 292477).

References

[1] Wei, Y., & Xu, Q. (2015). An overview of micro-force sensing techniques. Sensors and Actuators A: Physical, 234, 359-374.

[2] Krishna, G. M., & Rajanna, K. (2004). Tactile sensor based on piezoelectric resonance. IEEE sensors journal, 4(5), 691-697.

[3] Cotton, D. P., Chappell, P. H., Cranny, A., White, N. M., & Beeby, S. P. (2007). A novel thick-film piezoelectric slip sensor for a prosthetic hand. IEEE sensors journal, 7(5), 752-761.

[4] Lakhmi, R., Debéda, H., Dufour, I., & Lucat, C. (2010). Force sensors based on screen-printed cantilevers. IEEE Sensors Journal, 10(6), 1133-1137.

[5] Wenming, X., & Hui, Z. (2008, January). Bio-manipulation probe integration with micro-force sensor. In 2008 3rd IEEE International Conference on Nano/Micro Engineered and Molecular Systems (pp. 393-396). IEEE.

[6] Saketi, P., Latifi, S. K., Hirvonen, J., Rajala, S., Vehkaoja, A., Salpavaara, T., ... & Kallio, P. (2015). PVDF microforce sensor for the measurement of Z-directional strength in paper fiber bonds. *Sensors and Actuators A: Physical*, *222*, 194-203.

[7] Kim, K., Cheng, J., Liu, Q., Wu, X. Y., & Sun, Y. (2008, January). MEMS capacitive force sensors for micro-scale compression testing of biomaterials. In 2008 IEEE 21st International Conference on Micro Electro Mechanical Systems (pp. 888-891). IEEE.

[8] Qin, Y., Zhao, Y., & Wang, W. (2015, April). Development and characterization of three-axis micro-force sensor series. In 10th IEEE

International Conference on Nano/Micro Engineered and Molecular Systems (pp. 103-106). IEEE.
[9] Sasaki, D., Matsuura, K., Seta, H., Haraguchi, Y., Okano, T., & Shimizu, T. (2018). Contractile force measurement of human induced pluripotent stem cell-derived cardiac cell sheet-tissue. *PloS one*, *13*(5), e0198026.
[10] Wang, L., Dou, W., Malhi, M., Zhu, M., Liu, H., Plakhotnik, J., ... & Hamilton, R. (2018). Microdevice Platform for Continuous Measurement of Contractility, Beating Rate, and Beating Rhythm of Human-Induced Pluripotent Stem Cell-Cardiomyocytes inside a Controlled Incubator Environment. ACS applied materials & interfaces, 10(25), 21173-21183.
[11] Linder, P., Trzewik, J., Rüffer, M., Artmann, G. M., Digel, I., Kurz, R., ... & Artmann, A. T. (2010). Contractile tension and beating rates of self-exciting monolayers and 3D-tissue constructs of neonatal rat cardiomyocytes. Medical & biological engineering & computing, 48(1), 59.
[12] Mannhardt, I., Breckwoldt, K., Letuffe-Brenière, D., Schaaf, S., Schulz, H., Neuber, C., ... & Klampe, B. (2016). Human engineered heart tissue: analysis of contractile force. *Stem cell reports*, *7*(1), 29-42.
[13] Qu, Y., Zhao, F., Wang, X., Liu, J., Li, J., Song, Z., & Wang, Z. (2019). Cardiomyocyte contractile force changes in response to AGRWE detected by AFM. Micro & Nano Letters.
[14] Nagarajan, N., Vyas, V., Huey, B. D., & Zorlutuna, P. (2016). Modulation of the contractility of micropatterned myocardial cells with nanoscale forces using atomic force microscopy. Nanobiomedicine, 3, 1849543516675348.
[15] Pesl, M., Pribyl, J., Acimovic, I., Vilotic, A., Jelinkova, S., Salykin, A., ... & Rotrekl, V. (2016). Atomic force microscopy combined with human pluripotent stem cell derived cardiomyocytes for biomechanical sensing. Biosensors and Bioelectronics, 85, 751-757.
[16] Gaitas, A., Malhotra, R., Li, T., Herron, T., & Jalife, J. (2015). A device for rapid and quantitative measurement of cardiac myocyte contractility. Review of Scientific Instruments, 86(3), 034302.
[17] Virtanen, J., V. Sariola, and S. Tuukkanen. "Piezoelectric cantilever force sensor sensitivity measurements." *Journal of Physics: Conference Series*. Vol. 1065. No. 4. IOP Publishing, 2018.
[18] Badamasi, Y. A. (2014, September). The working principle of an Arduino. In 2014 11th International Conference on Electronics, Computer and Computation (ICECCO) (pp. 1-4). IEEE.
[19] D'Ausilio, A. (2012). Arduino: A low-cost multipurpose lab equipment. Behavior research methods, 44(2), 305-313.
[20] Jayetileke, H. R., De Mei, W. R., & Ratnayake, H. U. W. (2014, December). Real-time fuzzy logic speed tracking controller for a DC motor using Arduino Due. In 7th International Conference on Information and Automation for Sustainability (pp. 1-6). IEEE.
[21] Tibrewala, A., Hofmann, N., Phataralaoha, A., Jäger, G., & Büttgenbach, S. (2009). Development of 3D force sensors for nanopositioning and nanomeasuring machine. Sensors, 9(5), 3228-3239.
[22] Liang, Q., Zhang, D., Coppola, G., Wang, Y., Wei, S., & Ge, Y. (2014). Multi-dimensional MEMS/micro sensor for force and moment sensing: A review. IEEE Sensors Journal, 14(8), 2643-2657.
[23] Kan, T., Takahashi, H., Binh-Khiem, N., Aoyama, Y., Takei, Y., Noda, K., ... & Shimoyama, I. (2013). Design of a piezoresistive triaxial force sensor probe using the sidewall doping method. Journal of Micromechanics and Microengineering, 23(3), 035027.
[24] Microchip corporation, "SAM3X/SAM3A Series embedded 32-bit processor", ATSAM3X8E Data sheet, March 3 2015 [Revised March 23 2015]
[25] Virtanen J., Vehkaoja A., Tuukkanen S.. Piezoelectric dual axis cantilever sensor for dynamic low force measurements on an open source based platform , I3S2019
[26] Matsuya, Y., Uchimura, K., Iwata, A., Kobayashi, T., Ishikawa, M., & Yoshitome, T. (1987). A 16-bit oversampling A-to-D conversion technology using triple-integration noise shaping. IEEE Journal of Solid-State Circuits, 22(6), 921-929.
[27] Harpe, P., Cantatore, E., & van Roermund, A. (2014, February). 11.1 An oversampled 12/14b SAR ADC with noise reduction and linearity enhancements achieving up to 79.1 dB SNDR. In 2014 IEEE International Solid-State Circuits Conference Digest of Technical Papers (ISSCC) (pp. 194-195). IEEE.
[28] Shrout, T. R., & Zhang, S. J. (2007). Lead-free piezoelectric ceramics: Alternatives for PZT?. Journal of Electroceramics, 19(1), 113-126.
[29] Wolf, R. A., & Trolier-McKinstry, S. (2004). Temperature dependence of the piezoelectric response in lead zirconate titanate films. Journal of applied physics, 95(3), 1397-1406.
[30] Gubinyi, Z., Batur, C., Sayir, A., & Dynys, F. (2008). Electrical properties of PZT piezoelectric ceramic at high temperatures. Journal of Electroceramics, 20(2), 95-105.
[31] Fang, M., Rajput, S., Dai, Z., Ji, Y., Hao, Y., & Ren, X. (2019). Understanding the mechanism of thermal-stable high-performance piezoelectricity. Acta Materialia, 169, 155-161..

Juhani Virtanen received his M.Sc. (Tech) degree electronics and telecommunications engineering from Tampere University of Technology, Tampere, Finland in 1994. He has 20 years of industrial work experience in various positions. He is currently a doctoral student with research interests in sensor technology, measurements, physiological measurements and signal processing. He has 9 authored internationally peer reviewed articles and 7 internationally granted patents.

Arno Pammo received his B.Sc. (tech.) from Tampere University of Technology in 2016. Alongside of his master's studies in biomedical engineering, he has been working in research groups in the field of biomeasurements and renewable materials.

Antti Vehkaoja received his D.Sc. (Tech.) degree in automation science and engineering from Tampere University of Technology, Tampere, Finland in 2015. He has authored more than 70 scientific articles. He is currently an assistant professor (tenure tract) of sensor technology and biomeasurements at Tampere University. His research interests include development of embedded measurement technologies for physiological monitoring and related signal processing and data analysis methods with a focus on the assessment of vascular condition.

Sampo Tuukkanen received his P.hD. in applied physics from Department of Physics, University of Jyväskylä, Jyväskylä, Finland, in 2006. He is currently holding Associate Professor (tenure track) position at Tampere University, Tampere, Finland. His research interests are related to biomeasurements and bio-based devices. He has authored over 60 scientific articles, and having the h-index 19 (Google Scholar).